The Astrophysical Journal Supplement Series, 154:315–321, 2004 September

A GLIMPSE OF STAR FORMATION IN THE GIANT H II REGION RCW 49

B. A. Whitney,[1] R. Indebetouw,[2] B. L. Babler,[2] M. R. Meade,[2] C. Watson,[2] M. J. Wolff,[1] M. G. Wolfire,[3]
D. P. Clemens,[4] T. M. Bania,[4] R. A. Benjamin,[5] M. Cohen,[6] K. E. Devine,[2] J. M. Dickey,[7]
F. Heitsch,[8] J. M. Jackson,[4] H. A. Kobulnicky,[9] A. P. Marston,[10] J. S. Mathis,[2]
E. P. Mercer,[4] J. R. Stauffer,[11] S. R. Stolovy,[11] and E. Churchwell[2]
Received 2004 March 29; accepted 2004 May 13

ABSTRACT

GLIMPSE imaging using the Infrared Array Camera (IRAC) on the *Spitzer Space Telescope* indicates that star formation is ongoing in the RCW 9 giant H II region. A photometric comparison of the sources in RCW 49 to a similar area to its north finds that at least 300 stars brighter than 13th magnitude in band [3.6] have infrared excesses inconsistent with reddening due to foreground extinction. These are likely young stellar objects (YSOs) more massive than 2.5 $M_\odot$, suggesting that thousands more low-mass stars are forming in this cloud. Some of the YSOs are massive (B stars) and therefore very young, suggesting that a new generation of star formation is occurring, possibly triggered by stellar winds and shocks generated by the older (2–3 Myr) central massive cluster. The *Spitzer* IRAC camera has proven to be ideally suited for distinguishing young stars from field stars, and the GLIMPSE survey of the Galactic plane will likely find thousands of new star formation regions.

Subject headings: H II regions — infrared: general — infrared: stars — stars: formation — stars: pre–main-sequence

1. INTRODUCTION

RCW 49 is one of the most luminous and massive H II regions in the Galaxy. At its center lies the Westerlund 2 (hereafter W2; Westerlund 1960) compact cluster, which contains over a dozen OB stars and a Wolf-Rayet star; another Wolf-Rayet star lies several arcminutes away in the extended nebula (Moffat & Vogt 1975; Moffat et al. 1991; Carraro & Munari 2004; van der Hucht 2001). The age of the W2 cluster is estimated to be 2–3 Myr (Piatti et al. 1998). As discussed in Churchwell et al. (2004, hereafter C04), distance estimates range from ~2.5–8 kpc, and we follow their adoption of 4.2 kpc. At this distance, we estimate that the cluster luminosity is 1.4×10^7 $L_\odot$ on the basis of the *IRAS* flux and a relationship derived between far-infrared and bolometric luminosity (Hunter et al. 2000). The stellar mass is estimated to be $\sim3\times10^4$ $M_\odot$ from the radio-derived ionizing flux (Goss & Shaver 1970; Vacca et al. 1996)

The RCW 49 region was observed with the *Spitzer* (Werner et al. 2004) Infrared Array Camera (IRAC; Fazio et al. 2004) as part of the Galactic Legacy Infrared Mid-Plane Survey Extraordinaire (GLIMPSE; Benjamin et al. 2003) observing strategy validation. C04 presents IRAC images of this region that show highly structured, extended polycyclic aromatic hydrocarbon (PAH) and gas emission, extending out to ~12′ from the W2 cluster center. The PAH emission is likely excited by the strong ultraviolet/optical radiation from the central W2 cluster (Leger & Puget 1984; Allamandola et al. 1989), suggesting that large regions of the cloud are optically thin to the central cluster radiation. Furthermore, radio and infrared imaging show that at least the southwest part of the cloud is blown out (Whiteoak & Uchida 1997) (all directions in this paper are referred to in Galactic coordinates). Without detailed studies of the molecular gas in the RCW 49 region, it is unknown whether dense cores of gas and dust remain or whether the dust is optically thin. Has star formation ceased, and is the cloud in the process of disruption? Or is star formation ongoing, perhaps triggered by winds and shocks from the central cluster? This paper presents IRAC photometry of the RCW 49 region that reveals several hundred sources with large infrared excesses, likely indicating youth.

After discussing the observations in § 2, we present images of selected regions in § 3 and color-color and color-magnitude diagrams in § 4. In § 5 we show spectral energy distributions (SEDs) of two massive (B2) young stellar objects (YSOs). Section 6 concludes with a discussion of the current generation of star formation and how it may relate to the W2 cluster.

2. OBSERVATIONS

The observations are described in detail in C04. A $1\overset{\circ}{.}7\times0\overset{\circ}{.}7$ region was imaged 10 times with 1.2 s exposures in the four IRAC bands. We refer to these bands by their central wavelength in μm, i.e., [3.6], [4.5], [5.8], and [8.0]. The data were taken on 2003 December 23 (*Spitzer* PID 195) and were processed by the *Spitzer* Science Center (SSC) pipeline (version S9.0.1). Positional accuracies are better than 1″ (Werner et al. 2004). Point-source FWHM resolutions range from $\simeq1\overset{''}{.}6$ at [3.6] to $\simeq1\overset{''}{.}9$ at [8.0]. The data were further processed by the GLIMPSE pipeline (Benjamin et al. 2003): point sources

[1] Space Science Institute, 4750 Walnut Street, Suite 205, Boulder, CO 80301.
[2] Department of Astronomy, University of Wisconsin–Madison, 475 North Charter Street, Madison, WI 53706.
[3] Department of Astronomy, University of Maryland, College Park, MD 20742-2421.
[4] Institute for Astrophysical Research, Boston University, 725 Commonwealth Avenue, Boston, MA 02215.
[5] Physics Department, University of Wisconsin, 800 West Main Street, Whitewater, WI 53190.
[6] Radio Astronomy Laboratory, University of California-Berkeley, 601 Campbell Hall, Berkeley, CA 94720.
[7] Department of Astronomy, University of Minnesota, 116 Church Street SE, Minneapolis, MN 55455.
[8] Institute for Astronomy and Astrophysics, University of Munich, Scheinerstrasse 1, 81679 Munich, Germany.
[9] Department of Physics and Astronomy, University of Wyoming, P.O. Box 3905, Laramie, WY 82072.
[10] ESTEC/SCI-SA, Postbus 299, 2200 AG Noordwijk, Netherlands.
[11] *Spitzer* Science Center, California Institute of Technology, MC 314-6, Pasadena, CA 91125.

were extracted from each frame using a modified version of DAOPHOT (Stetson 1987) and cross-referenced using the SSC band merger. We produced a catalog of all sources detected at least eight of 10 times in any of the four IRAC bands. For the present study, we culled the catalog to include only those sources with signal-to-noise ratios greater than 10 in any band. We estimate the photometric errors from simulations by placing point sources on a realistic background (using the RCW 49 diffuse flux after stars are subtracted out) and comparing the processed photometry to the input values. The rms errors are <0.05 mag in bands [3.6] and [4.5] for sources brighter than 13 and 12.5 mag, respectively, and <0.07 mag in band [5.8] and <0.15 mag in band [8.0] for sources brighter than 11.7 mag. Only sources brighter than these magnitudes (in a given band) are displayed in the color-color and color-magnitude diagrams in § 4. The flux calibration was checked against five early A-type dwarf stars and agrees to within 7% in all IRAC bands with the calculated fluxes (Cohen et al. 2003; Kurucz 1993).

3. ZONES OF STAR FORMATION

Figure 1 (Plate 1) shows a three-color image mosaic[12] at K_s, [3.6], and [4.5] μm (the K_s-band image is a mosaic of Two Micron All Sky Survey [2MASS][13] images). The [3.6] band diffuse emission (*green*) is dominated by PAHs and small grains, the [4.5] emission (*red*) is mostly hydrogen Brα and small grains (C04), and the K_s-band (*blue*) is likely Brγ and perhaps dust scattering. Main-sequence stars appear blue in these images. The boxed regions in Figure 1 are shown to larger scale in Figure 2 (Plate 2).

The top left panel of Figure 2 shows the W2 cluster. This cluster contains five O7 V stars, one O6 V star, and a WN7 star (Moffat et al. 1991). The bright star about 1′ northwest of the cluster marked by the arrow is an O7 supergiant (Moffat et al. 1991). Winds from the W2 cluster have produced for a radio ring about 4′ in radius centered on the cluster (Whiteoak & Uchida 1997). The second region (region 2) is 3.′4 southwest of the W2 center. As discussed in § 5, the bright red source and diffuse green source (marked) are likely massive (B3) YSOs. This cluster resides (in projection) in the ''blow-out'' region of the RCW 49 nebula, where the radio ring is disrupted and winds and UV radiation are probably escaping (Whiteoak & Uchida 1997; C04, Fig. 1). The third highlighted region, at 4.′3 southeast of W2, contains a column of material similar to the elephant trunks of M16 (Hester et al. 1996). The red star at the tip of the elephant trunk is a strong IR emitter, and the bright red star to the southeast is likely a massive YSO since it has similar flux and colors to the two sources discussed in § 5. To the north at the edge of the image lies the second known Wolf-Rayet star in the RCW 49 nebula (Moffat et al. 1991). It is thought to be responsible for a second radio bubble (Whiteoak & Uchida 1997). The fourth region is located 7.′7 southeast of W2. It contains several faint, red sources and dark lanes. Region 5 is located 7′8 east of W2, and region 6 is located 9′1 south of W2; each contains a small group of red sources. Region 6 is located on the perimeter of the blow-out region.

These images of clustered red sources and dark lanes suggest that star formation is taking place throughout the RCW 49 nebula. We next examine stellar photometry of the entire region to determine whether this is indeed the case.

4. COLOR-COLOR AND COLOR-MAGNITUDE DIAGRAMS

Figure 3 shows color-color plots of the RCW 49 region (*green circles*) and a ''field'' region of similar area about 0.°75 to the north (*pink circles*) centered at (l, b) = (284.°18, 0.°41). The black cross at upper right in each panel shows typical error bars for each color sequence.

The black arrows show reddening vectors derived from optical/near-IR extinction studies of the diffuse interstellar medium (Cardelli et al. 1989), and the gray arrows show reddening vectors derived from this data set (Indebetouw et al. 2004. Note that the length of the arrows in the top left panel represent an optical extinction of $A_V = 3$, whereas the length of the arrows in the other three panels show $A_V = 30$. The black symbols represent colors from models of 1 million year old sources (using Siess et al. 2000 evolutionary tracks for central source temperatures and luminosity) surrounded by varying amounts of circumstellar gas and dust (10^{-4} to 10 $M_\odot$).

The models were computed using a radiative transfer code that calculates emission from envelopes, disks, and outflows surrounding stars (Whitney et al. 2003). The model central star masses are 2.5, 3.8, and 5.9 $M_\odot$, corresponding to luminosities of 10 $L_\odot$ (*filled circles*), 100 $L_\odot$ (*crosses*), and 730 $L_\odot$ (*open triangles*).

The 2MASS catalog was used to create the near-IR color sequence in the top left panel of Figure 3. Only stars brighter than 14th magnitude in all three bands are plotted since the errors increase below this. The near-IR color sequence is typical of a star formation region. The field stars (*pink*) follow the reddening line. The stars that are very red or below the reddening line are usually classified as IR excess sources with disks or envelopes. However, many IR excess sources lie along the reddening line and are difficult to distinguish from reddened main-sequence stars. In contrast, the other panels in Figure 3 using IRAC data show that infrared-excess sources in RCW 49 are well separated from field stars, which generally have a small color range.

Comparing the colors of the RCW 49 stars to the field stars, we find that 357 stars out of 1393 in RCW 49 have colors $[3.6]-[4.5]>0.2$, $[4.5]-[5.8]>0.35$, or $[5.8]-[8.0]>0.2$ mag compared with 21/1114 in the field (about 2%). We note that because of our conservative brightness limits for this initial study, many of the faint stars apparent in the images in Figure 2 are not included in the color-color plots. Even so, it is likely that at least 300 of the sources in this data set are surrounded by warm circumstellar dust, which indicates that they have recently formed or are in the process of formation.

Figure 4 shows color-magnitude diagrams of the RCW 49 region (*green circles*) and the northern field (*pink*). The model symbols (*black*) are as described in Figure 3. The width of the field star distribution matches reasonably well to the error bars at upper right. The horizontal dashed line in each panel shows the expected brightness of a B5 main-sequence star at a distance of 4.2 kpc (synthesized from the 2–35 μm spectra of Cohen 1993). On the basis of the number of YSOs more luminous than this (about 300), and assuming a fairly standard initial mass function (IMF; Cox 2000, p. 488), we estimate the total number of YSOs to be $\sim$7000 and their total mass to be $\sim$4500 $M_\odot$.

[12] Mosaics were created using Montage software, funded by the National Aeronautics and Space Administration's Earth Science Technology Office.

[13] The Two Micron All Sky Survey is a joint project of the University of Massachusetts and the Infrared Processing and Analysis Center/California Institute of Technology, funded by the National Aeronautics and Space Administration and the National Science Foundation.

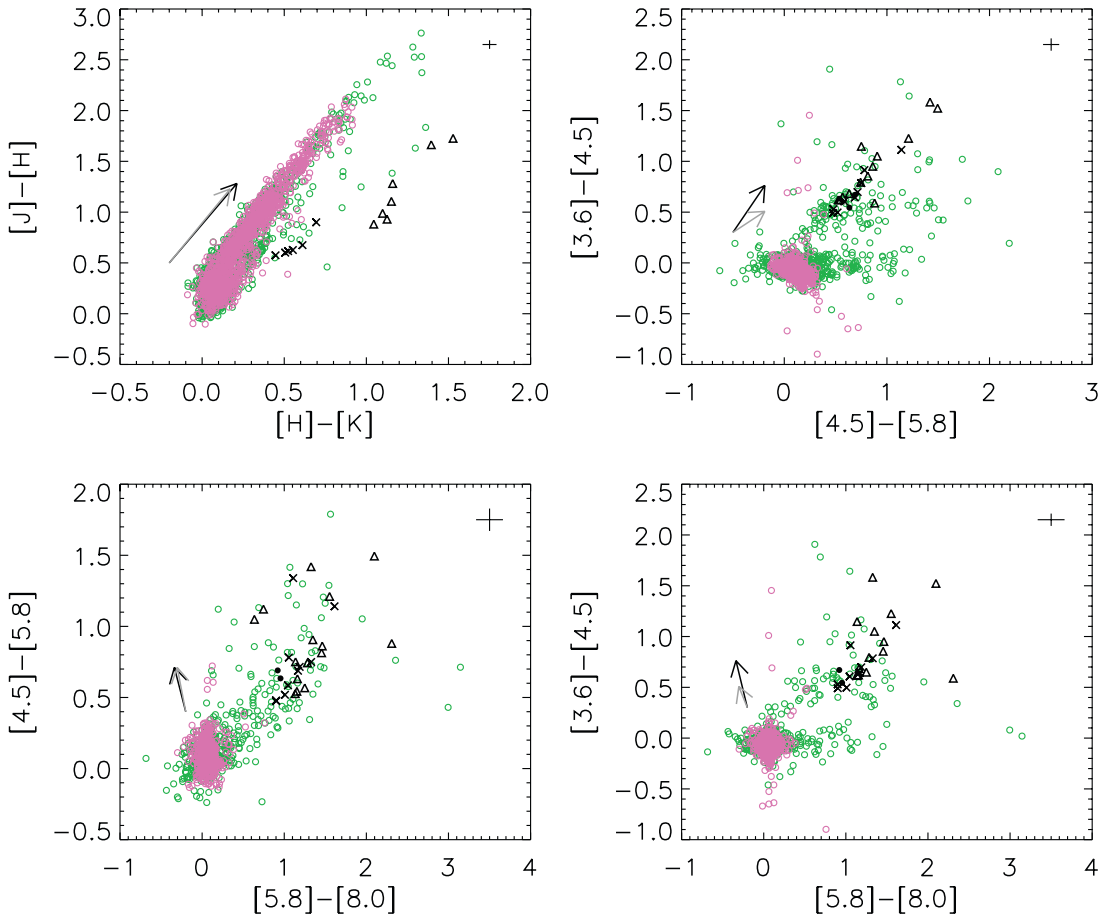

FIG. 3.—Color-color plots. The black and gray arrows show the reddening vectors for two different extinction laws (see text). Sources from the RCW 49 nebula are shown in green, and those from an off-cloud region are shown in pink. Typical error bars are shown at upper right of each panel. YSO models of various masses are also shown as black symbols (*open triangles:* 5.9 $M_{\odot}$; *crosses:* 3.8 $M_{\odot}$; *filled circles:* 2.5 $M_{\odot}$).

Where is most of the star formation occurring in this cloud? Figure 5 plots the fraction of red sources as a function of radius from the W2 cluster center, where red is defined as $[3.6]-[4.5]>0.2$, $[4.5]-[5.8]>0.35$, and $[5.8]-[8.0]>0.3$ mag (based on the color-magnitude diagrams of Fig. 4). This distribution peaks within about $4'$ ($\sim$2 pc) from the W2 cluster center and decreases beyond that. The diffuse emission has a similar distribution (C04, Fig. 3), suggesting the possibility of a systematic bias toward finding red stars due to higher [5.8] and [8.0] backgrounds. However, the density of total stars (of all colors) as a function of radius is fairly constant beyond about $2'$, suggesting that we are seeing the entire population of stars above our magnitude limits. The correlation between the red stars and the diffuse flux is probably real and due to higher diffuse flux in regions of higher star formation activity. We conclude from this plot that star formation is occurring preferentially within about $4'$ ($\sim$5 pc) from the W2 cluster center and decreases beyond that. Interestingly, this is the approximate outer radius of the radio ring (Whiteoak & Uchida 1997) and the "plateau region" of the diffuse flux (C04, Fig. 3) where it is thought that winds and radiation have swept up and compressed gas and dust. This may have produced conditions for a second generation of star formation. Since the medium is not smooth, the induced star formation likely occurs over a range of radii. The YSOs in region 2 (Figs. 1 and 2) and the elephant trunk in region 3 fall within this region. Interestingly, the YSOs in region 6 lie on the edge of the blow-out cavity. However, regions 4 and 5 are well beyond the radio ring and may represent a more quiescent form of star formation.

5. SEDs OF SELECTED SOURCES

In this section, we present SEDs of just two of the many interesting sources in the RCW 49 nebula. These are in region 2 of Figure 2, marked by arrows. The observed SEDs include data from 2MASS, *Spitzer* IRAC, and the *Midcourse Space Experiment* (*MSX*).[14] The source indicated by the left arrow in region 2 is the brightest source in the region and is mildly saturated at IRAC [5.8] and [8.0] bands. The source shown by the right arrow is a triangular greenish object. The SEDs of both sources are shown in Figure 6. IRAC photometry of the bright source was done by our automated pipeline. We did aperture photometry of the triangular source over a $4''$ aperture. The flux at $\lambda > 8$ μm from these sources is blended at *MSX* resolution ($18''$), although likely dominated by the source at left.

It is clear from the brightness of these sources that they are luminous and likely of high mass. We computed model SEDs for the YSOs using the code of Whitney et al. (2003). Alvarez et al. (2004) modeled near-IR scattered light images of massive YSOs using the same geometries we use to fit the SEDs in

[14] This publication makes use of data products from the *Midcourse Space Experiment*. Processing of the data was funded by the Ballistic Missile Defense Organization with additional support from NASA Office of Space Science.

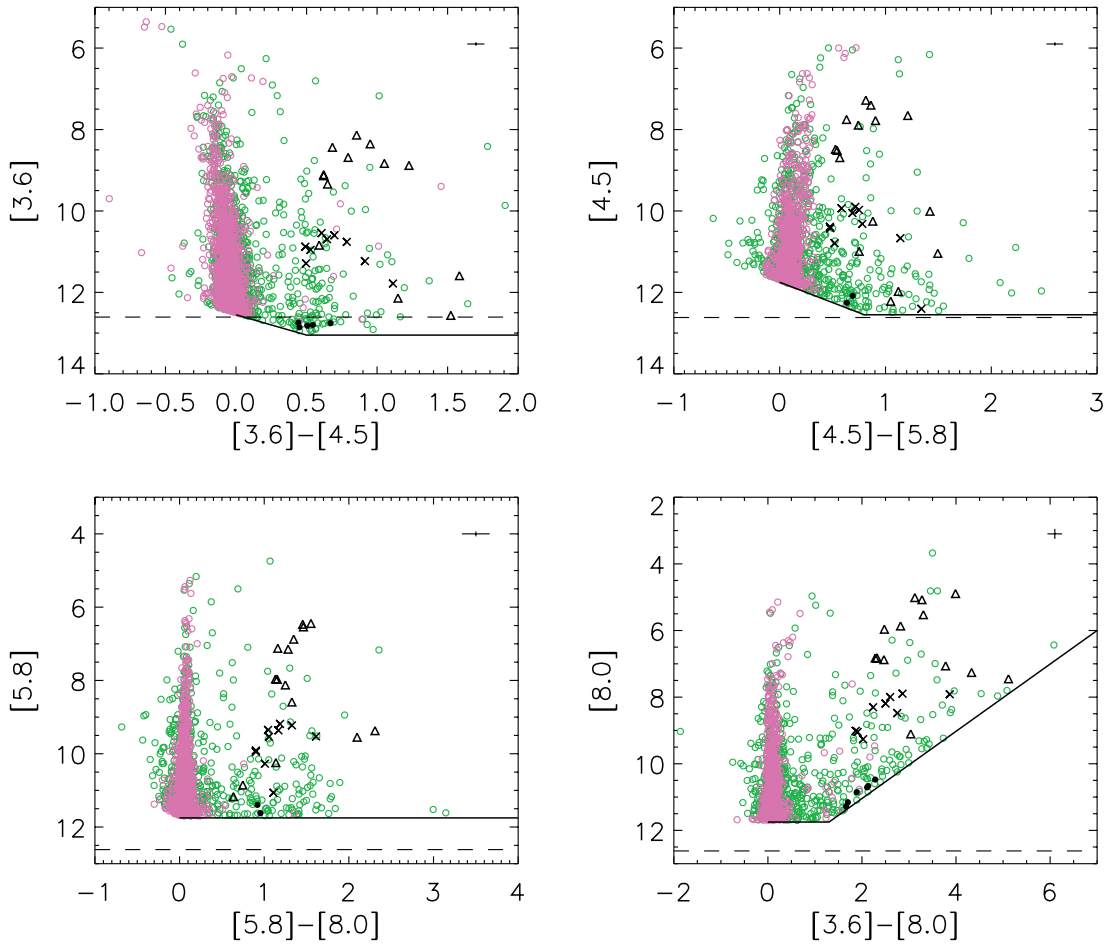

FIG. 4.—Color-magnitude diagrams. They symbols are as described in Fig. 3. The dashed line shows the magnitude of a B5 main-sequence star at 4.2 kpc. The solid lines show the envelope created by the magnitude limits of the source list. Typical error bars are shown at top right of each panel.

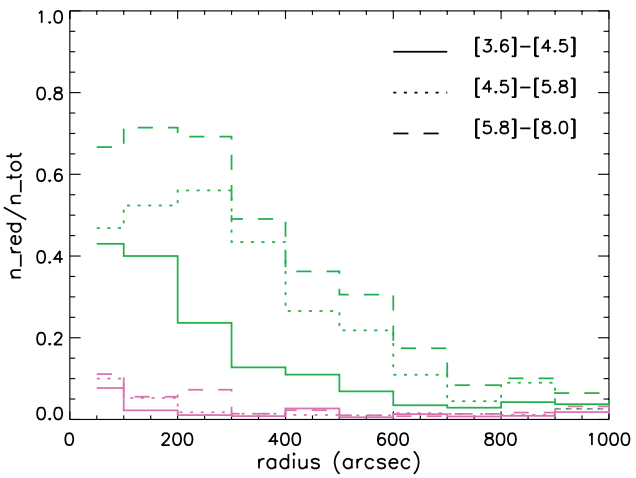

FIG. 5.—Green lines show the fraction of red stars as a function of radius in RCW 49 for three IRAC colors. The pink lines show the fraction of red stars as a function of radius for the field 0.°75 north of RCW 49.

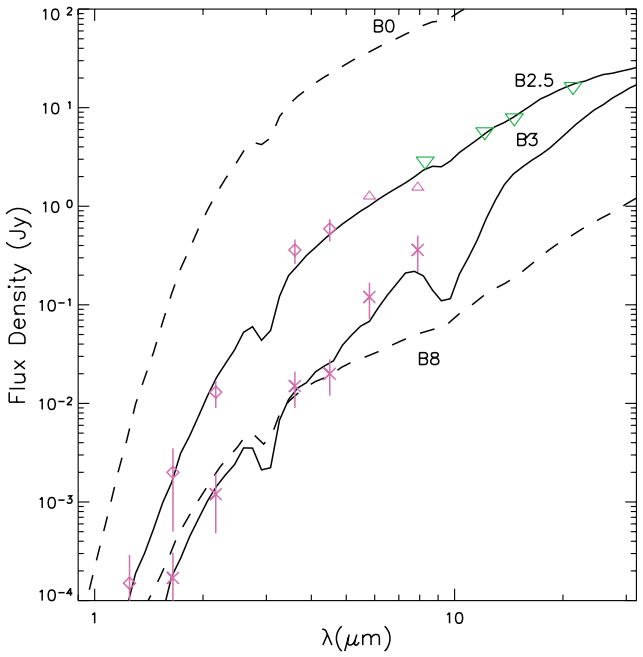

FIG. 6.—SEDs for the two marked YSOs in region 2 (see Fig. 2). The bright YSO (Fig. 2, *left arrow*) is indicated by pink diamonds with error bars and upward-pointing triangles in the saturated bands. The triangular YSO (right arrow in Fig. 2) is shown as pink crosses with error bars. The *MSX* points are shown as green downward-pointing triangles. Models are shown for embedded YSOs with various central source spectral types, all at inclination 70°.

Figure 6: rotationally flattened infalling envelopes, disks, and dust-filled outflow cavities. The model that fits the bright source SED best is powered by a B2 main-sequence star and has an envelope with an infall rate of $2.7 \times 10^{-5}\ M_{\odot}\ \mathrm{yr}^{-1}$ and a disk radius of 500 AU; this gives an envelope extinction along the line of sight of $A_V = 30$. The model that fits the triangular source is powered by a B2.5 star and has an infall rate of $8 \times 10^{-5}\ M_{\odot}\ \mathrm{yr}^{-1}$, disk radius of 100 AU, and envelope extinction of 200 along the line of sight. Both models are viewed at an inclination of $i = 70^{\circ}$(where pole-on is defined as $i = 0^{\circ}$), and have foreground extinctions of $A_V = 15$. The SEDs could probably be fitted with other envelope structures as long as a substantial amount of dust resides close to the star, and therefore the stars are sufficiently young that very little dust clearing has occurred.

6. CONCLUSIONS

The large number of infrared excess sources in RCW 49 indicates that star formation is ongoing in this giant H II region. We find that at least 300 stars brighter than 13th magnitude in the [3.6] band are pre–main-sequence or young stars of mass $\gtrsim 2.5\ M_{\odot}$.

On the basis of integration of a standard IMF, we conclude that the YSOs in the RCW 49 complex comprise a stellar mass of $\sim 4500\ M_{\odot}$. If the YSOs represent a second generation of star formation, this suggests that the mass of the second generation is about 15% of the first. The presence of YSOs of B spectral type does indeed suggest that some star formation is very recent. Whether it is continuous or triggered by the W2 cluster is uncertain. The apparent excess of star formation near the radio/IR ring (Fig. 1) and several of the sites of star formation near the ring and blowout region perimeters (regions 2, 3, and 6 in Fig. 2) suggest that energy input from W2 may have triggered recent star formation. On the other hand, regions 4 and 5 appear to be forming stars in a relatively quiescent region of the cloud.

The detailed nature of the star formation in RCW 49—whether triggered or continuous, clustered or distributed—and the spatial distribution of mass requires further study by the wider astronomical community. The images of this field have been released with the opening of the public archive; the GLIMPSE catalog and mosaic images will be available to the community from the *Spitzer* Science Center in the fall of 2004.

We are grateful to Stephan Jansen for his invaluable work maintaining the GLIMPSE computing network. Support for this work, part of the *Spitzer Space Telescope* Legacy Science Program, was provided by NASA through contracts 1224653 (Univ. Wisconsin, Madison), 1225025 (Boston Univ.), 1224681 (Univ. Maryland), 1224988 (Space Science Inst.), 1242593 (Univ. California, Berkeley), 1253153 (Univ. Minnesota), 11253604 (Univ. Wyoming), and 1256801 (Univ. Wisconsin, Whitewater) by the Jet Propulsion Laboratory, California Institute of Technology, under NASA contract 1407.

REFERENCES

Allamandola, L. J., Tielens, A. G. G. M., & Barker, J. R. 1989, ApJS, 71, 733
Alvarez, C., Hoare, M., & Lucas, P. 2004, A&A, 419, 203
Benjamin, R. A., et al. 2003, PASP, 115, 953
Cardelli, J. A., Clayton, G. C., & Mathis, J. S. 1989, ApJ, 345, 245
Carraro, G., & Munari, U. 2004, MNRAS, 347, 625
Churchwell, E., et al. 2004, ApJS, 154, 322 (C04)
Cohen, M. 1993, AJ, 105, 1860
Cohen, M., Megeath, S. T., Hammersley, P. L., Martín-Luis, F., & Stauffer, J. 2003, AJ, 125, 2645
Cox, A. N. 2000, Allen's Astrophysical Quantities (New York: AIP)
Fazio, G., et al. 2004, ApJS, 154, 10
Goss, W. M., & Shaver, P. A. 1970, Australian J. Phys. Astrophys. Suppl., 14, 1
Hester, J. J., et al. 1996, AJ, 111, 2349
Hunter, T. R., Churchwell, E., Watson, C., Cox, P., Benford, D. J., & Roelfsema, P. R. 2000, AJ, 119, 2711
Indebetouw, R., et al. 2004. ApJ, submitted
Kurucz, R. 1993, CD-ROM 13, ATLAS9 Stellar Atmosphere Programs and 2 km/s grid (Cambridge: SAO), 13
Leger, A., & Puget, J. L. 1984, A&A, 137, L5
Moffat, A. F. J., Shara, M. M., & Potter, M. 1991, AJ, 102, 642 (MSP)
Moffat, A. F. J., & Vogt, N. 1975, A&AS, 20, 125
Piatti, A. E., Bica, E., & Claria, J. J. 1998, A&AS, 127, 423
Siess, L., Dufour, E., & Forestini, M. 2000, A&A, 358, 593
Stetson, P. B. 1987, PASP, 99, 191
Vacca, W. D., Garmany, C. D., & Shull, M. J. 1996, ApJ, 460, 914
van der Hucht, K. 2001, NewA Rev., 45, 135
Werner, M. W., et al. 2004, ApJS, 154, 1
Westerlund, B. 1960, Ark. Astron., 2, 419
Whiteoak, J. B. Z., & Uchida, K. I. 1997, A&A, 317, 563
Whitney, B. A., Wood, K., Bjorkman, J. E., & Cohen, M. 2003, ApJ, 598, 1079

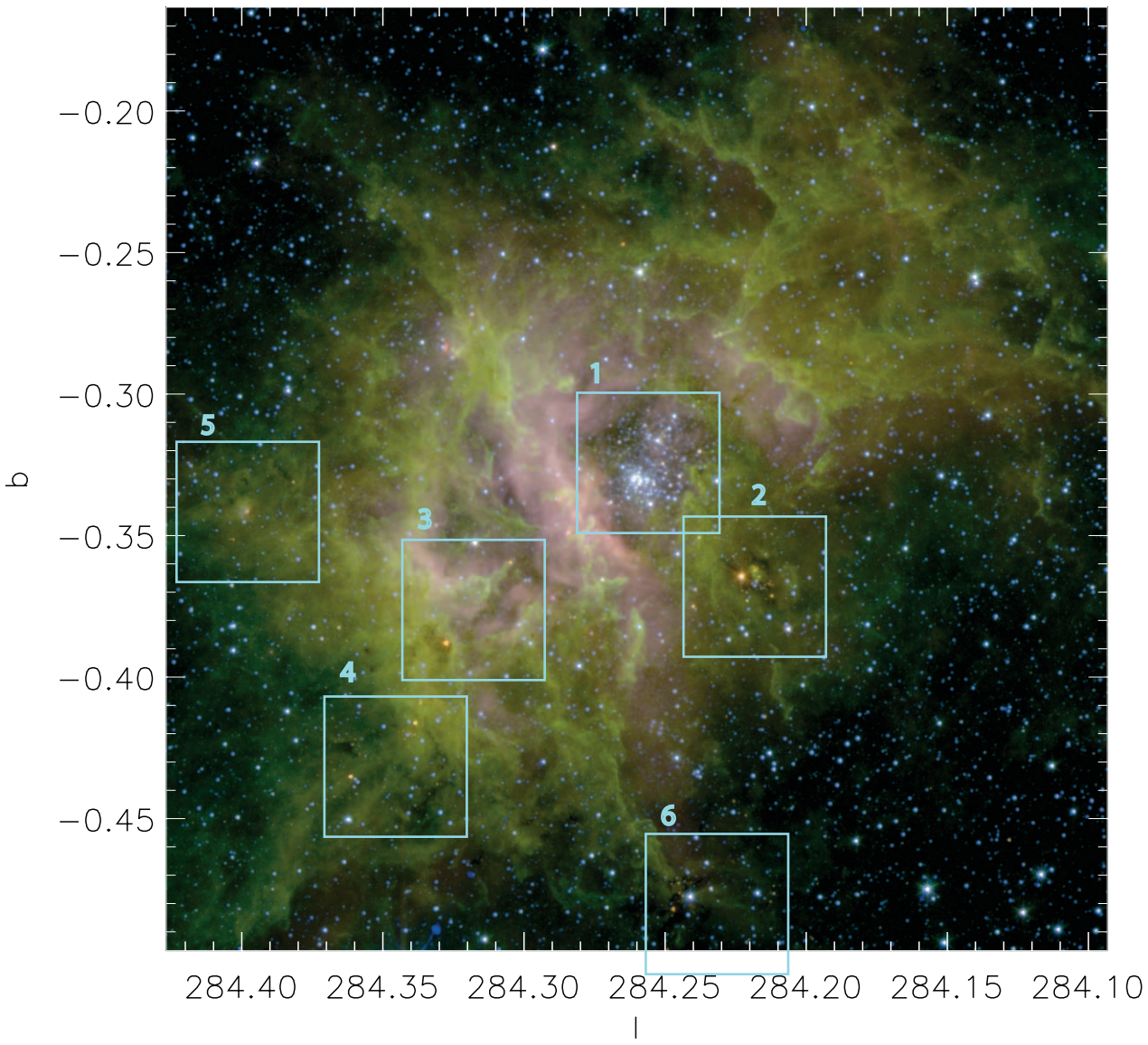

FIG. 1.—Three-color composite image of the RCW 49 region. The K_s image is displayed as blue, [3.6] as green, and [4.5] as red. The images are scaled logarithmically. The blue boxes mark the regions shown in Fig. 2.

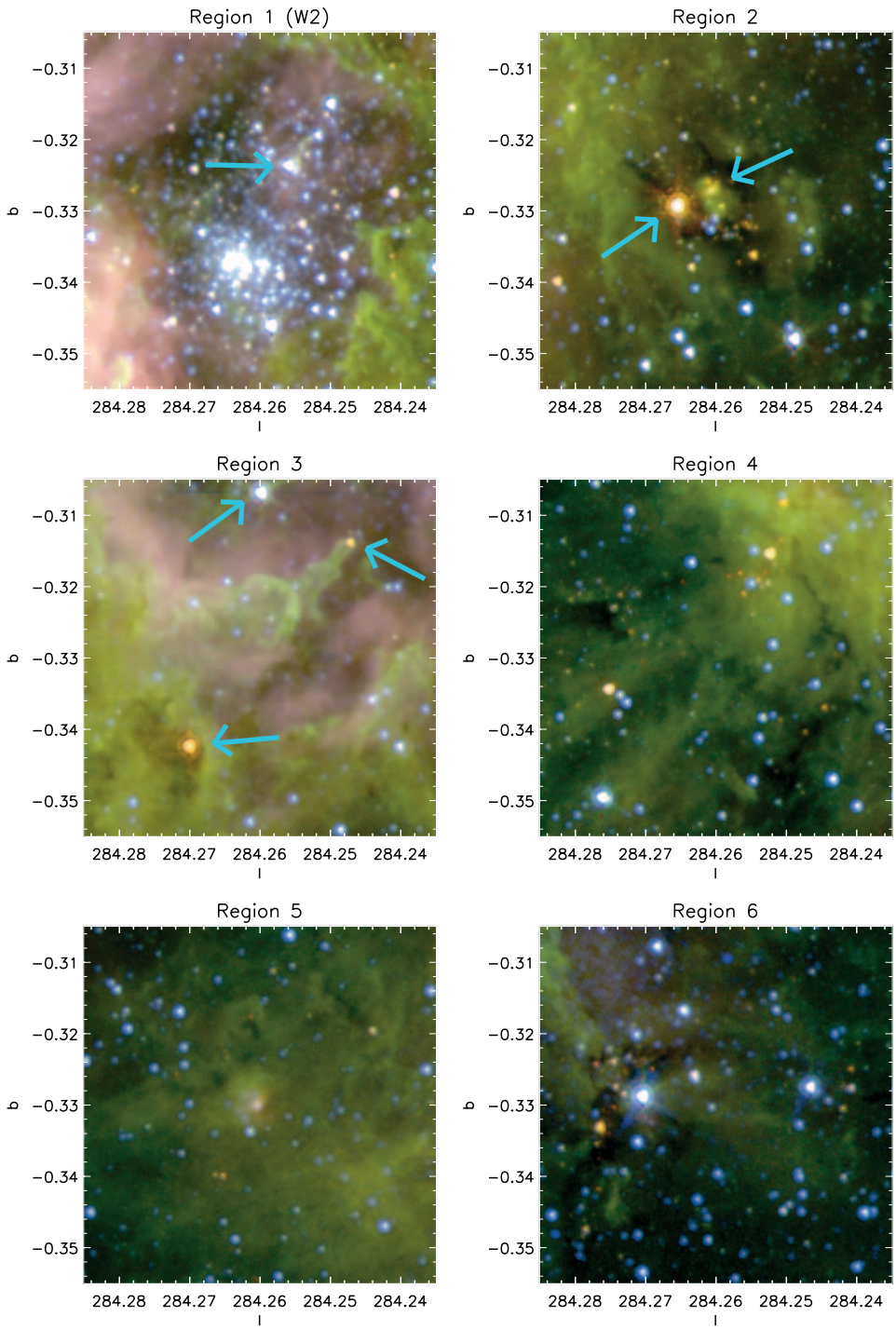

FIG. 2.—K_s-[3.6]-[4.5] three-color composite images of selected regions (the marked boxes in Fig. 1). Each image is 3′ on a side. Arrows mark sources discussed in the text.